M&C 2017 - International Conference on Mathematics & Computational Methods Applied to Nuclear Science & Engineering, Jeju, Korea, April 16-20, 2017, on USB (2017)

A Residual-based *A Posteriori* Estimator of the Spatial Approximation Error for Discrete Ordinates Solutions of the Transport Equation

Nathan H. Hart, Yousry Y. Azmy

Department of Nuclear Engineering, North Carolina State University,
3140 Burlington Engineering Labs, 2500 Stinson Drive, Raleigh, NC, USA 27695-7909
nhhart@ncsu.edu, yyazmy@ncsu.edu

Abstract - *We introduce an a posteriori spatial discretization error estimator for the discrete ordinates transport equation. We estimate the residual and invert the discrete transport operator using the residual as a source to estimate the error. This is compared to the true error calculated via the Method of Manufactured Solutions as well as the estimated error as given by Ragusa and Wang.*

I. INTRODUCTION

Spatially discretizing the discrete ordinates approximation of the radiation transport equation results in a departure from the spatially continuous solution quantified by a discretization error. If this discretization error is known exactly, the true solution of the spatially continuous equation projected onto the discrete mesh can be found. Practically, of course, the discretization error is not known exactly, meaning the error must be estimated.

Unlike in Monte Carlo methods where errors or uncertainties in the solution are always reported to indicate the statistical quality of the estimated solution, deterministic solutions are rarely accompanied by estimated discretization errors, likely due to unproven usefulness. However, error estimators and indicators – estimators that are intended to estimate the behaviour of the error rather than the error itself, but may or may not estimate the error well – have provided uses beyond pure estimation of the solution error. One use for error estimators is calculating a reliable upper bound on the spatial discretization error of a solution [1]. The most common use for spatial discretization error estimators and indicators is to drive adaptive mesh refinement, a process in which the discrete domain, or select subsections of it, are refined based on the estimated error in each cell.

O'Brien and Azmy posited that an *a posteriori* method of inverting the discrete transport operator on an estimated residual could return an error estimation as good as the residual estimation – i.e., a perfect residual estimation will return the exact error [2]. We show the validity of this approach, introduce a residual estimator that is mathematically consistent, and compare this new method with established estimators.

II. THEORY

1. Radiation Transport Equation

In this work, the steady-state, one-speed radiation transport equation is solved on the domain $D \in [0, X] \times [0, Y]$ contained in boundary ∂D. The angular discretization method used in this work is the discrete ordinates (S_N) method.

$$\vec{\Omega}_n \cdot \nabla\psi_n(x,y) + \sigma_t\psi_n(x,y) = \sigma_s\phi(x,y) + q(x,y),\ (x,y) \in D,\ n = 1, ..., N, \quad (1)$$

$$\psi_n(x,y) = \psi_{BC,n},\ (x,y) \in \partial D,\ \hat{n} \cdot \vec{\Omega}_n < 0. \quad (2)$$

Equations 1 and 2 show the complete transport equation as used in this work, where the scalar flux is defined as $\phi(x,y) \equiv \sum_{n=1}^{N} w_n\psi_n(x,y)$. The angular nodes and weights, w_n, $n = 1, ..., N$, are calculated using Level Symmetric quadrature, outlined in [3], although the methods outlined in this work are applicable to all discrete ordinate quadrature methods.

Scattering is treated isotropically because this is all our Method of Manufactured Solutions (MMS) reference solution generator allows for, although there is no reason to believe that the estimators presented in this work are limited to isotropic scattering. The same is true of the homogeneous treatment of cross sections. Additionally, restrictions on MMS limit this work to fixed boundary conditions. We believe the modifications to this work to account for albedo or periodic boundary conditions would be minor, though we would no longer have the luxury of exact solutions provided by MMS for comparison.

2. Method of Manufactured Solutions

The Method of Manufactured Solutions is used to generate a radiation transport problem for which the true continuous spatial solution is known [4] in order to benchmark and evaluate with exact certainty the quality of a discretization method. In the particular MMS that we employ, material properties across the domain are constant, and the combined volumetric source $Q(x,y)$ – the sum of the fixed external source and the scattering source, Eq. 3 – is also fixed and constant.

$$Q = Q(x,y) \equiv q(x,y) + \sigma_s\phi(x,y) = const. \quad (3)$$

Due to the fixed properties throughout the domain the spatially continuous transport equation can be solved with no approximation (in space) using the Method of Characteristics, Eq. 4.

$$\psi_n(x,y) = \begin{cases} \psi_{<B,T>,n}(x - sign(\mu_n)|\frac{\mu_n}{\eta_n}|\bar{y})e^{\frac{-\sigma_t}{|\eta_n|}\bar{y}} \\ \qquad + \frac{Q}{\sigma_t}(1 - e^{\frac{-\sigma_t}{|\eta_n|}\bar{y}}), & \bar{y} < |\frac{\eta_n}{\mu_n}|\bar{x}, \\ \psi_{<R,L>,n}(y - sign(\eta_n)|\frac{\eta_n}{\mu_n}|\bar{x})e^{\frac{-\sigma_t}{|\mu_n|}\bar{x}} \\ \qquad + \frac{Q}{\sigma_t}(1 - e^{\frac{-\sigma_t}{|\mu_n|}\bar{x}}), & \bar{y} > |\frac{\eta_n}{\mu_n}|\bar{x}, \end{cases} \quad (4)$$

where $\bar{x} = \frac{1-sign(\mu_n)}{2}X + sign(\mu_n)x$ and $\bar{y} = \frac{1-sign(\eta_n)}{2}Y + sign(\eta_n)y$. To use MMS as a reference solution, the scattering source portion of the combined source is subtracted from Q and used as a fixed source input for the discrete problem:

$$q(x,y) = Q - \sigma_s \sum_{n=1}^{N} w_n \psi_n(x,y). \quad (5)$$

Boundary conditions (BC's) and the combined source term are chosen to ensure a positive fixed source [5]. In each transport problem (with one exception) there exists one singular characteristic (SC) per ordinate emanating from the origin of the transport sweep with a slope of η_n/μ_n. The SC is significant because across this line the true, spatially continuous transport solution has an irregularity of the same order as that where the boundaries meet. This is illustrated in Table I, where it can be seen that for a C^0 solution, a solution which has jump discontinuities along the SC, the boundary conditions differ. Note that $< B,T >$ subscripts refer to the bottom and top boundaries while $< R,L >$ refers to the right and left. However, when the

TABLE I: BC's corresponding to continuity across SC

	$\psi_{<B,T>,n}$	$\psi_{<R,L>,n}$
C^0	0	$(Q-\sigma_s)/\sigma_s$
C^1	0	0

boundary conditions are the same this only results in a C^1 solution, in which the first order derivatives have discontinuities along the SC; this is because the derivative at the discontinuity is unbounded. By defining higher order derivatives of the boundary conditions, arbitrarily high degrees of continuity across the SC can be had, including infinite. However real-world applications are limited to only C^0 and C^1, so these are the only regularity orders considered in this work.

3. Discontinuous Galerkin Finite Element Method

All spatially discrete approximated transport solutions in this work are calculated using the Discontinuous Galerkin Finite Element Method of order Λ (DGFEM-Λ), where Λ is the highest order spatial moment calculated in the numerical method. DGFEM approximates the solution as a truncated expansion of coefficients multiplying basis functions,

$$\psi_n^{(h)}(x,y) = \sum_{k=0}^{\Lambda}\sum_{l=0}^{\Lambda} \psi_{n,k,l} v_{k,l}(x,y), \quad (6)$$

where moments of the solution in discrete subcells $K_{i,j} \in [x_{i-1}, x_i] \times [y_{j-1}, y_j]$ with boundaries $\partial K_{i,j}$, where $i = 1, ..., N_x$ and $j = 1, ..., N_y$, are found through integration as follows:

$$\psi_{n,k,l}^{(i,j)} = \frac{1}{\Delta x \Delta y} \int_{K_{i,j}} v_{k,l}(x,y)\psi_n^{(h)}(x,y)dA, \quad \text{for } k,l = 0, ..., \Lambda. \quad (7)$$

Moments of other functions are found analogously. In this work $\Delta x = XN_x^{-1}$ and $\Delta y = YN_y^{-1}$ are both constant and proportional, so a generic Δ will often be used when discussing order of accuracy. Because it is a discontinuous method, solution values on the subcell boundaries must be defined as existing on either the external (+) or internal (−) traces. A trace is defined as the limit of the value at coordinates that approach the cell boundary either from outside the cell (external) or inside the cell (internal) [4].

The DGFEM-Λ method gives the following discrete transport equation:

$$\begin{aligned}
&\mu_n[\langle v^{(i,j)}(x_i^+, y), \psi_n^{(i,j)}(x_i^-, y)\rangle_y - \langle v^{(i,j)}(x_{i-1}^+, y), \psi_n^{(i,j)}(x_{i-1}^-, y)\rangle_y] \\
&+\eta_n[\langle v^{(i,j)}(x, y_j^+), \psi_n^{(i,j)}(x, y_j^-)\rangle_x - \langle v^{(i,j)}(x, y_{j-1}^+), \psi_n^{(i,j)}(x, y_{j-1}^-)\rangle_x] \\
&- \mu_n(\frac{\partial v^{(i,j)}}{\partial x}, \psi_n^{(i,j)}(x,y)) - \eta_n(\frac{\partial v^{(i,j)}}{\partial y}, \psi_n^{(i,j)}(x,y)) \\
&+ (v^{(i,j)}, \sigma_t \psi_n^{(i,j)}(x,y)) = (v^{(i,j)}, \sigma_s\phi(x,y) + q(x,y)). \quad (8)
\end{aligned}$$

In this context $\langle f(\xi), g(\xi)\rangle_\xi = \int_{\Delta\xi} f(\xi)g(\xi)d\xi$ and $(f(\xi,\eta), g(\xi,\eta)) = \int_{\Delta\xi}\int_{\Delta\eta} f(\xi,\eta)g(\xi,\eta)d\xi d\eta$, where ξ and η are generic spatial variables. The test functions are given as:

$$v_{k,l}(x,y) = P_k(\tilde{x})P_l(\tilde{y}), \text{ for } k,l = 0, ..., \Lambda, \quad (9)$$

where $P_k(x)$ is the Legendre Polynomial of order k. The variables $\tilde{x}$ and $\tilde{y}$ are transformed spatial variables about the cell center, $\tilde{x} = \frac{2(x-x_c)}{\Delta x}$ and $\tilde{y} = \frac{2(y-y_c)}{\Delta y}$. This work will focus on the DGFEM-0 approximation, Eq. 10, although this could be generalized to higher order Λ,

$$\begin{aligned}
&\mu_n\Delta y[\psi_{n,0,0}^{(i,j)} - \psi_{n,0,0}^{(i-1,j)}] + \eta_n\Delta x[\psi_{n,0,0}^{(i,j)} - \psi_{n,0,0}^{(i,j-1)}] \\
&+ \sigma_t\Delta x\Delta y\psi_{n,0,0}^{(i,j)} = \Delta x\Delta y[\sigma_s\phi_{0,0}^{(i,j)} + q_{0,0}^{(i,j)}]. \quad (10)
\end{aligned}$$

The definition of DGFEM-Λ is important to show because the high-order approximations to be considered in the future will have a different form as the order is increased.

MMS solutions are projected onto the discrete domain in a manner analogous to Eq. 7, allowing for direct comparison when calculating the true error as well as the various estimators. The Source Iteration (SI) method is used to converge the DGFEM solution, although conceivably any iteration method should be consistent with the methods used in this work. The iterations are converged to 10^{-10} to ensure validity of the error comparisons presented below.

4. The Residual Source Estimator

Equation 1 in the domain D can be rewritten as

$$L\psi = \mathcal{S}\psi + q, \quad (11)$$

where L represents the continuous streaming plus total-collision operator (the left-hand side of Eq. 1), $\mathcal{S}$ is the scattering operator, q is the continuous fixed source, and ψ is the true, continuous solution to the transport equation. Equation 8 on a mesh with cell size 'h' can be rewritten as

$$L_h\psi^{(h)} = \mathcal{S}\psi^{(h)} + q_h, \quad (12)$$

where L_h represents the discrete transport operator (the left-hand side of Eq. 8), q_h is the continuous fixed source projected

onto the discrete domain, and $\psi^{(h)}$ is the solution to the discrete transport equation that approximates the continuous transport equation. Here, we define the residual R as the additional term that exists when the true solution to the continuous transport equation projected onto the domain, referred to as $[\psi]_h$, is inserted into Eq. 12,

$$R \equiv \mathcal{S}[\psi]_h + q_h - L_h[\psi]_h. \tag{13}$$

The spatial discretization error is defined as $\varepsilon \equiv \psi^{(h)} - [\psi]_h$, and, recognizing that the scattering and discrete transport operators are linear and that $q_h = -\mathcal{S}\psi^{(h)} + L_h\psi^{(h)}$, we can rearrange terms and get the following equation for the error,

$$L_h\varepsilon = \mathcal{S}\varepsilon + R \tag{14}$$

Equation 14 can be solved using the same iterative method used to obtain the solution to the discrete transport equation. The goal of this work is to accurately estimate this residual *a posteriori* and, by extension, the error without any knowledge of the true solution. The validity of this approach is examined in a later section.

5. Defining Error and Error Norms

Because the error is an angular quantity and piecewise continuous in space, we apply two norms in order to collapse it into a discrete scalar quantity. Scalar quantities are preferable because they are easier to work with and are more applicable to adaptive mesh refinement. The first norm we define as the local "angular L_2 norm", or $e^{(i,j)}_{ang.}$, Eq. 15. It is called "angular" because it emphasizes the difference in the angular flux.

$$e^{(i,j)}_{ang.} \equiv \left(\sum_n w_n \int_{K_{i,j}} \varepsilon_n^2 dA\right)^{1/2} = \left(\sum_n w_n \int_{K_{i,j}} (\psi_n^{(h)} - \psi_n)^2 dA\right)^{1/2}. \tag{15}$$

The other norm is the local "scalar L_2 norm", or $e^{(i,j)}_{sca.}$, Eq. 16. It is called "scalar" because it emphasizes the difference in the scalar flux.

$$e^{(i,j)}_{sca.} \equiv \left(\int_{K_{i,j}} (\sum_n w_n\varepsilon_n)^2 dA\right)^{1/2} = \left(\int_{K_{i,j}} (\phi^{(h)} - \phi)^2 dA\right)^{1/2}. \tag{16}$$

These local norms can easily be modified to be global norms. When an uppercase 'E' is used it indicates that the error norm being presented is the true error norm computed directly from DGFEM and MMS solutions, whereas a lowercase 'e' indicates the error norm has been calculated via an error estimate. In this work, the error's accuracy is generally presented using the local "effectivity index", Eq. 17,

$$\theta^{(i,j)}_{ang./sca.} \equiv \left|\frac{e^{(i,j)}_{ang./sca.}}{E^{(i,j)}_{ang./sca.}}\right|. \tag{17}$$

A global effectivity index can be calculated with the global norms analogously.

6. The Ragusa-Wang Estimator

Various works ([2],[6],[7]) have shown empirically that the two-mesh difference-based estimator introduced by Ragusa and Wang in [7] generally estimates the true error better than the other estimators and indicators it has been compared against. For this reason we use the Ragusa-Wang estimator as the primary comparison for the residual source estimator developed in this work. The Ragusa-Wang estimator essentially uses a solution on a uniformly refined mesh, designated with superscript '$h/2$', as a reference solution. The Ragusa-Wang estimator as defined in [7] is given in Eq. 18,

$$e^{RW} \equiv \frac{\int_{K_{i,j}} (\phi^{(h)} - \phi^{(h/2)})^2 dA}{\int_D \phi_h dA}. \tag{18}$$

To keep the estimator consistent with this work, we redefine the Ragusa-Wang estimator using the same norms introduced previously,

$$e^{RW(i,j)}_{ang.} \equiv \left(\sum_n w_n \int_{K_{i,j}} (\psi_n^{(h)} - \psi_n^{(h/2)})^2 A\right)^{1/2}, \tag{19}$$

$$e^{RW(i,j)}_{sca.} \equiv \left(\int_{K_{i,j}} (\phi^{(h)} - \phi^{(h/2)})^2 dA\right)^{1/2}. \tag{20}$$

The scope of this work does not include any analysis into the computational costs of the Ragusa-Wang estimator versus the residual source estimator.

III. RESULTS & ANALYSIS

A suite of MMS problems is used to assess the estimators' accuracy in this work. The domain in all problems was square, and S_4 level-symmetric quadrature was used. The SI stopping criterion was $\|\phi_{new} - \phi_{old}\|_\infty \leq 10^{-10}$.

1. Conceptual Validation of the Residual Source Estimator

As a proof of concept for the residual source estimator the MMS solutions are used to find exact residuals. This is done by projecting the MMS solution onto the mesh and directly calculating the residual via Eq. 13. By using this residual as a fixed source for the DGFEM-0 solver, we were able to solve for the true error as calculated by $\varepsilon = \psi^{(h)} - [\psi]_h$ exactly.

Figure 1 highlights the features of the true residual. On boundary cells the residual is orders of magnitude larger than the residual in the domain. Also, on cells intersected by the singular characteristic and cells immediately downwind from those cells the residual is orders of magnitude greater. This is because DGFEM-0 fails to capture the discontinuity in the true solution along the SC's. Cells immediately downwind from cells intersected by the SC are affected because the flux in the cell intersected by the SC is used in finding the flux in the downwind cell, see Eq. 10. We also empirically find that the leading order terms of cell-wise convergence of the residual are $O(\Delta)$ when in the domain, shown in Figure 2, and $O(1)$ (converges to a constant value as the mesh refines) when on the boundary or SC, shown in Figures 3 and 4.

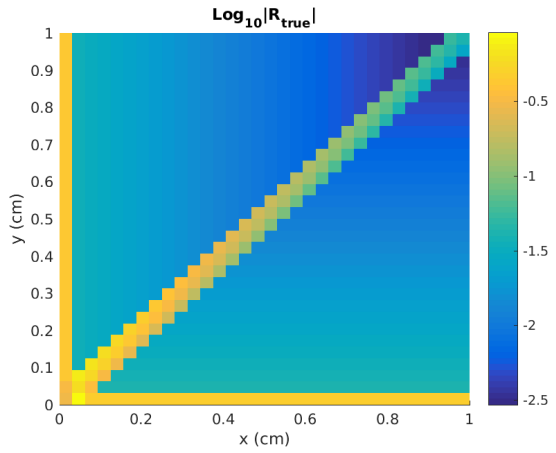

Fig. 1: True residual for $\mu_n = \eta_n = 0.35002$ ordinate; C^0 irregularity along the SC, $\sigma_t = 1.0$, $c = 0.9$, $N_x = N_y = 32$

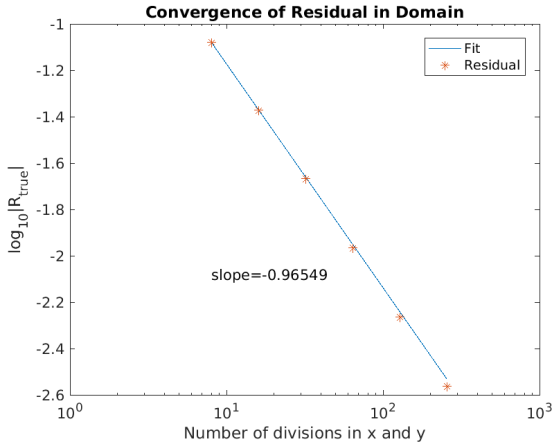

Fig. 2: Residual convergence with mesh refinement

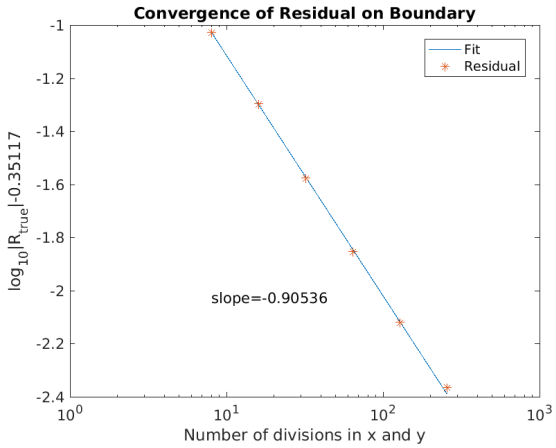

Fig. 3: Boundary cell residual convergence with mesh refinement

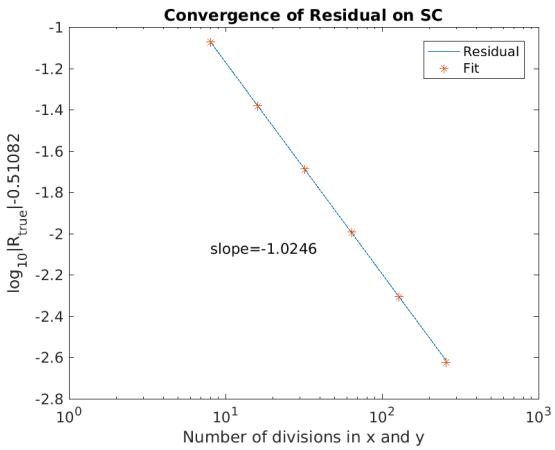

Fig. 4: SC residual convergence with mesh refinement

2. Approximating the Residual

Generally, the true solution is not known, so we approximate it using an $O(\delta^3)$ Taylor expansion about the origin of cell $K_{i,j}$ (note the partial derivative notation $\frac{\partial f}{\partial x} = f^x$),

$$\psi_n(x_i + \delta_x, y_j + \delta_y) \approx \psi_n(x_i, y_j) + \delta_x \psi_n^x(x_i, y_j) + \delta_y \psi_n^y(x_i, y_j) + \frac{\delta_x^2}{2}\psi_n^{xx}(x_i, y_j) + \delta_x\delta_y\psi_n^{xy}(x_i, y_j) + \frac{\delta_y^2}{2}\psi_n^{yy}(x_i, y_j). \quad (21)$$

From here we will drop the discrete ordinate subscript n, and no mesh superscript implies the quantity is evaluated at (x_i, y_j). Equation 21 corresponds to the Legendre moment,

$$\psi_{0,0}^{(i,j)} \approx \psi + \frac{\Delta x}{2}\psi^x + \frac{\Delta y}{2}\psi^y + \frac{\Delta x^2}{6}\psi^{xx} + \frac{\Delta x \Delta y}{4}\psi^{xy} + \frac{\Delta y^2}{6}\psi^{yy}. \quad (22)$$

The Legendre moment in the preceding x-direction cell is

$$\psi_{0,0}^{(i-1,j)} \approx \psi - \frac{\Delta x}{2}\psi^x + \frac{\Delta y}{2}\psi^y + \frac{\Delta x^2}{6}\psi^{xx} - \frac{\Delta x \Delta y}{4}\psi^{xy} + \frac{\Delta y^2}{6}\psi^{yy}, \quad (23)$$

and the Legendre moment in the preceding y-direction cell is

$$\psi_{0,0}^{(i,j-1)} \approx \psi + \frac{\Delta x}{2}\psi^x - \frac{\Delta y}{2}\psi^y + \frac{\Delta x^2}{6}\psi^{xx} - \frac{\Delta x \Delta y}{4}\psi^{xy} + \frac{\Delta y^2}{6}\psi^{yy}. \quad (24)$$

These approximations are accurate up to $O(\Delta^3)$, except for when the cell is intersected by a SC. Moments of the scattering source and fixed source are identical to Eq. 22. Knowing that in the absence of SC's, DGFEM-0 will converge with $O(\Delta)$ [8], we seek an expression for the residual using these moments that is accurate up to $O(\Delta^2)$. This is as simple as plugging Eq.'s 22-24 into Eq. 10 and cancelling like terms, then the

remaining terms are equal to the residual. The (i, j) superscript for the residual indicates that this is cell-wise residual.

$$R^{(i,j)} \approx -\{[\sigma_t\psi+\mu\psi^x+\eta\psi^y-(\sigma_s\phi+q)]+\sigma_t(\frac{\Delta x}{2}\psi^x+\frac{\Delta y}{2}\psi^y) + (\mu\frac{\Delta y}{2}+\eta\frac{\Delta x}{2})\psi^{xy}-\frac{\Delta x}{2}(\sigma_s\phi^x+q^x)-\frac{\Delta y}{2}(\sigma_s\phi^y+q^y)\} = -\{\sigma_t(\frac{\Delta x}{2}\psi^x+\frac{\Delta y}{2}\psi^y)+(\mu\frac{\Delta y}{2}+\eta\frac{\Delta x}{2})\psi^{xy} - \frac{\Delta x}{2}(\sigma_s\phi^x+q^x)-\frac{\Delta y}{2}(\sigma_s\phi^y+q^y)\}. \quad (25)$$

The term in Eq. 25 contained in the square brackets is equal to zero, since this is merely Eq. 1 rearranged. The remainder is the residual on the interior cells accurate to $O(\Delta^2)$. Also we see that the leading order term in the residual is $O(\Delta)$, which is in agreement with the empirically observed interior cell residual convergence. However, the residual on a boundary cell does not use the same expression, since the boundary flux is known from the BC's. The expressions for residuals on boundary cells, denoted by a $[B]$ superscript, are given by:

$$R^{([B],j)} = -\{\frac{\mu}{\Delta x}[\psi^{([B],j)}_{0,0}-\psi_{<R,L>}]+\frac{\eta}{\Delta y}[\psi^{([B],j)}_{0,0}-\psi^{([B],j-1)}_{0,0}] + \sigma_t\psi^{([B],j)}_{0,0}-\sigma_s\phi^{([B],j)}_{0,0}-q^{([B],j)}_{0,0}\} \approx -\{\frac{\mu}{\Delta x}[\psi+\frac{\Delta x}{2}\psi^x+\frac{\Delta y}{2}\psi^y+ \frac{\Delta x^2}{6}\psi^{xx}+\frac{\Delta x\Delta y}{4}\psi^{xy}+\frac{\Delta y^2}{6}\psi^{yy}-\psi_{<R,L>}] + \frac{\eta}{\Delta y}[\Delta y\psi^y+\frac{\Delta x\Delta y}{2}\psi^{xy}]+\sigma_t[\psi+\frac{\Delta x}{2}\psi^x+\frac{\Delta y}{2}\psi^y] - [\sigma_s\phi+q+\frac{\Delta x}{2}(\sigma_s\phi^x+q^x)+\frac{\Delta y}{2}(\sigma_s\phi^y+q^y)]\}.$$

Terms are cancelled and rearranged to give

$$R^{([B],j)} \approx -\{[\mu\psi^x+\eta\psi^y+\sigma_t\psi_{<R,L>}-(\sigma_s\phi+q)] + \mu[-\frac{1}{2}\psi^x+\frac{\Delta y}{2\Delta x}\psi^y+\frac{\Delta x}{6}\psi^{xx}+\frac{\Delta y}{4}\psi^{xy}+\frac{\Delta y^2}{6\Delta x}\psi^{yy}]+ \eta\frac{\Delta x}{2}\psi^{xy}+\sigma_t[\frac{\Delta x}{2}\psi^x+\frac{\Delta y}{2}\psi^y]-[\frac{\Delta x}{2}(\sigma_s\phi^x+q^x)+\frac{\Delta y}{2}(\sigma_s\phi^y+q^y)]\}.$$

The first term on the right-hand side is equal to zero. Since the source is typically undefined on the boundaries, but does exist on the interior trace of a boundary cell, we substitute derivatives for angular flux quantities – i.e., $(\sigma_s\phi^x+q^x) = \sigma_t\psi^x+\mu\psi^{xx}+\eta\psi^{xy}$,

$$R^{([B],j)} \approx -\{\mu[-\frac{1}{2}\psi^x+\frac{\Delta y}{2\Delta x}\psi^y+\frac{\Delta x}{6}\psi^{xx}+\frac{\Delta y}{4}\psi^{xy}+\frac{\Delta y^2}{6\Delta x}\psi^{yy}] + \eta\frac{\Delta x}{2}\psi^{xy}+\sigma_t[\frac{\Delta x}{2}\psi^x+\frac{\Delta y}{2}\psi^y]-\frac{\Delta x}{2}[\sigma_t\psi^x+\mu\psi^{xx}+\eta\psi^{xy}] - \frac{\Delta y}{2}[\sigma_t\psi^y+\mu\psi^{xy}+\eta\psi^{yy}]\}.$$

Combining like terms gives Eq. 26, where a bar indicates that the value is known directly from the BC's,

$$R^{([B],j)} \approx -\{\mu[-\frac{1}{2}\psi^x+\frac{\Delta y}{2\Delta x}\bar{\psi}^y - \frac{\Delta x}{3}\psi^{xx}-\frac{\Delta y}{4}\psi^{xy}+\frac{\Delta y^2}{6\Delta x}\bar{\psi}^{yy}]-\eta\frac{\Delta y}{2}\bar{\psi}^{yy}\}. \quad (26)$$

A similar process for the top and bottom boundary cells as well as the corner cells gives

$$R^{(i,[B])} \approx -\{-\mu\frac{\Delta x}{2}\bar{\psi}^{xx}+\eta[\frac{\Delta x}{2\Delta y}\bar{\psi}^x - \frac{1}{2}\psi^y+\frac{\Delta x^2}{6\Delta y}\bar{\psi}^{xx}-\frac{\Delta x}{4}\psi^{xy}-\frac{\Delta y}{3}\psi^{yy}]\}, \quad (27)$$

and

$$R^{([B],[B])} \approx -\{\mu[-\frac{1}{2}\bar{\psi}^x+\frac{\Delta y}{2\Delta x}\bar{\psi}^y-\frac{\Delta x}{3}\bar{\psi}^{xx}-\frac{\Delta y}{4}\bar{\psi}^{xy}+\frac{\Delta y^2}{6\Delta x}\bar{\psi}^{yy}] + \eta[\frac{\Delta x}{2\Delta y}\bar{\psi}^x-\frac{1}{2}\bar{\psi}^y+\frac{\Delta x^2}{6\Delta y}\bar{\psi}^{xx}-\frac{\Delta x}{4}\bar{\psi}^{xy}-\frac{\Delta y}{3}\bar{\psi}^{yy}]\}. \quad (28)$$

These residual expressions are $O(\Delta^2)$ accurate so long as the true angular flux quantities are known. These expressions converge to a constant with $O(\Delta)$, which is in agreement with our empirically observed boundary residual convergence. Note that while all derivatives that appear in the corner cell residual expression are known exactly, the corner cell by definition is intersected by an SC.

Figure 5 shows that the derived Taylor-expansion-approximated (TE) residual expressions accurately capture the true residual, and we have observed that the leading error term is $O(\Delta^2)$, in accordance with theory. An exception to this is on the SC where the discontinuities in the angular flux and higher order derivatives are not adequately approximated by the Taylor expansion. Figure 6 shows the angular L_2 effec-

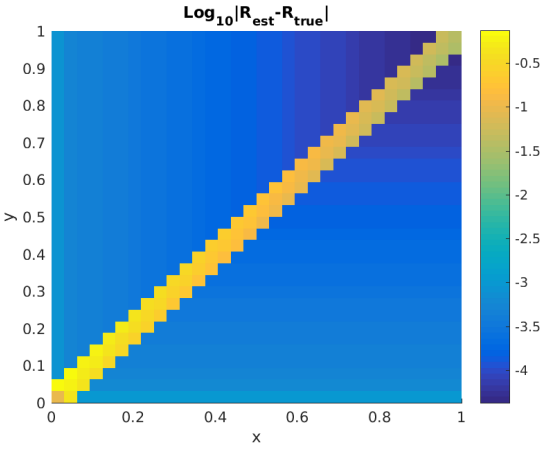

Fig. 5: TE residual minus true residual for $\mu_n = \eta_n = 0.35002$ ordinate; C^0 irregularity along the SC, $\sigma_t = 1.0$, $c = 0.9$, $N_x = N_y = 32$

tivity across the domain. The TE residual-estimated error is accurate in regions untainted by the SC. However, near the SC's and especially in regions where the SC's intersect the estimated error under or overestimates. Intuitively this makes sense, since, as shown in Fig. 1, the true residual is orders of magnitude higher on the SC than in the domain, and since our expressions do not capture the behaviour of the solution along the SC's appropriately (see Fig. 5), the estimated residual and, by extension, the estimated error would logically be inaccurately estimated.

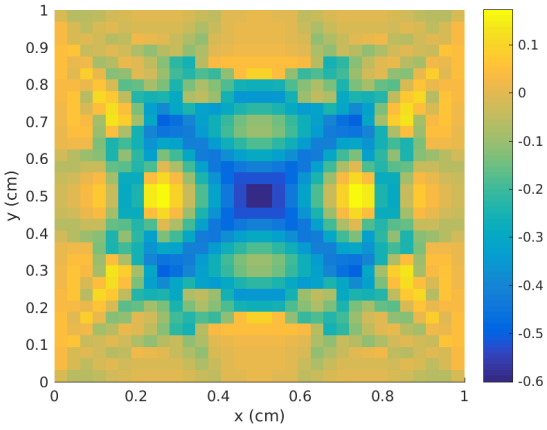

Fig. 6: $\log_{10}$-scale angular L_2 effectivity for TE residual-estimated error; C^0 irregularity along the SC, $\sigma_t = 1.0$, $c = 0.9$, $N_x = N_y = 32$

Another observation is that as the optical thickness (σ_t) of the problem is increased, the TE residual deviates from the true residual. This is understandable because the spatial gradient of the true solution will be higher and the Taylor expansion approximation worse. However, the effect this has on the estimated error is minor compared to that of poor approximation on the SC's.

3. Estimating Derivatives with DGFEM-0 Quantities

In the DGFEM-0 approximation, the angular flux is approximated as a piecewise constant function in space, meaning that all derivatives are undefined (in fact, all derivatives order $\Lambda+1$ and higher are undefined for a general DGFEM-Λ approximation). This means that all derivative terms in the residual expressions must be approximated using order 0 terms. On the interior cells this is straightforward. The desired flux terms are located on cell corners, where the flux is discontinuous due to the DGFEM-0 approximation. The angular flux moments in each cell in terms of the same Taylor series used to derive the residual equations are given:

$$\psi_{0,0}^{(i,j)} = \psi + \frac{\Delta x}{2}\psi^x + \frac{\Delta y}{2}\psi^y + \frac{\Delta x^2}{6}\psi^{xx} + \frac{\Delta x\Delta y}{4}\psi^{xy} + \frac{\Delta y^2}{6}\psi^{yy} + O(\Delta^3), \tag{29}$$

$$\psi_{0,0}^{(i-1,j)} = \psi - \frac{\Delta x}{2}\psi^x + \frac{\Delta y}{2}\psi^y + \frac{\Delta x^2}{6}\psi^{xx} - \frac{\Delta x\Delta y}{4}\psi^{xy} + \frac{\Delta y^2}{6}\psi^{yy} + O(\Delta^3) \tag{30}$$

$$\psi_{0,0}^{(i,j-1)} = \psi + \frac{\Delta x}{2}\psi^x - \frac{\Delta y}{2}\psi^y + \frac{\Delta x^2}{6}\psi^{xx} - \frac{\Delta x\Delta y}{4}\psi^{xy} + \frac{\Delta y^2}{6}\psi^{yy} + O(\Delta^3), \tag{31}$$

$$\psi_{0,0}^{(i-1,j-1)} = \psi - \frac{\Delta x}{2}\psi^x - \frac{\Delta y}{2}\psi^y + \frac{\Delta x^2}{6}\psi^{xx} + \frac{\Delta x\Delta y}{4}\psi^{xy} + \frac{\Delta y^2}{6}\psi^{yy} + O(\Delta^3). \tag{32}$$

The two first order angular flux derivatives as well as the cross derivative that appear in the interior cell residual expression can be approximated by,

$$\psi^x = \frac{1}{2\Delta x}(\psi_{0,0}^{(i,j)} - \psi_{0,0}^{(i-1,j)} + \psi_{0,0}^{(i,j-1)} - \psi_{0,0}^{(i-1,j-1)}) + O(\Delta^2), \tag{33}$$

$$\psi^y = \frac{1}{2\Delta y}(\psi_{0,0}^{(i,j)} - \psi_{0,0}^{(i,j-1)} + \psi_{0,0}^{(i-1,j)} - \psi_{0,0}^{(i-1,j-1)}) + O(\Delta^2), \tag{34}$$

$$\psi^{xy} = \frac{1}{\Delta x\Delta y}(\psi_{0,0}^{(i,j)} - \psi_{0,0}^{(i-1,j)} - \psi_{0,0}^{(i,j-1)} + \psi_{0,0}^{(i-1,j-1)}) + O(\Delta). \tag{35}$$

The scalar flux derivative is calculated analogously. However, the continuous function of the fixed source should be known exactly, so its derivatives need not be approximated. On the boundaries the estimation of the same derivatives is nearly analogous, except some values in the expressions are known directly from the BC's (denoted by a bar). For example, on the x-boundary the flux moments in the boundary cells are given by a Taylor series in Eq. 36:

$$\begin{aligned}\psi_{0,0}^{([B],j)} &= \bar{\psi} + \frac{\Delta x}{2}\psi^x + \frac{\Delta y}{2}\bar{\psi}^y + \frac{\Delta x^2}{6}\psi^{xx} + \frac{\Delta x\Delta y}{4}\psi^{xy} + \frac{\Delta y^2}{6}\bar{\psi}^{yy} + O(\Delta^3),\\ \psi_{0,0}^{([B],j-1)} &= \bar{\psi} + \frac{\Delta x}{2}\psi^x - \frac{\Delta y}{2}\bar{\psi}^y + \frac{\Delta x^2}{6}\psi^{xx} - \frac{\Delta x\Delta y}{4}\psi^{xy} + \frac{\Delta y^2}{6}\bar{\psi}^{yy} + O(\Delta^3).\end{aligned} \tag{36}$$

Immediately the issue with estimating derivatives on the boundaries is seen, namely that there are three unknowns and two equations. To remedy this we must reduce the order of accuracy of our Taylor expansion and estimate the first order derivative accuracy,

$$\psi^x = \frac{1}{\Delta x}(\psi_{0,0}^{([B],j)} + \psi_{0,0}^{([B],j-1)} - 2\bar{\psi}) + O(\Delta). \tag{37}$$

However, this means that our residual approximation on the boundary cells is only $O(\Delta)$ accurate.

The approximated-derivative (AD) residual is calculated by substituting approximate *a posteriori* derivative expressions (Eqs. (24)-(26),(28)) for the true derivatives in the TE residual equations. The moments used in approximating the derivatives come from the DGFEM-0 transport solution, not the MMS solution, meaning that this residual relies *only* on the numerical solution. Figure 7 shows the difference between the AD residual and the true residual in the domain. Here we see that the AD residual estimation is significantly worse than the TE residual estimation. The SC estimation is once again the poorest in the domain, and, as the mesh is refined, the SC's in other ordinates begin to appear in the corresponding plot due

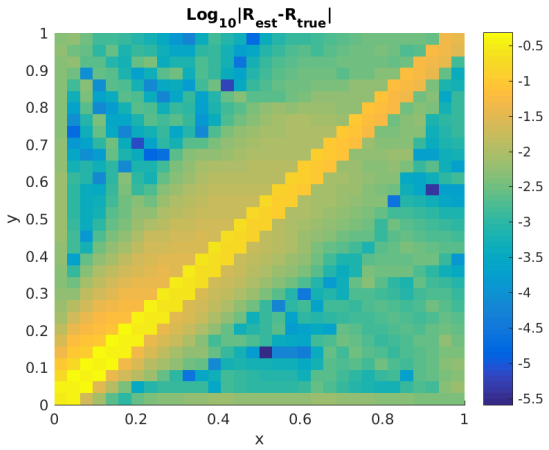

Fig. 7: AD residual minus true residual for $\mu_n = \eta_n = 0.35002$ ordinate; C^0 irregularity along the SC, $\sigma_t = 1.0$, $c = 0.9$, $N_x = N_y = 32$

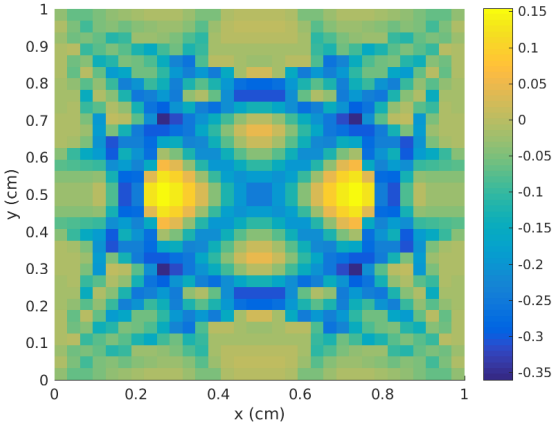

Fig. 8: $\log_{10}$-scale angular L_2 effectivity for AD residual-estimated error; C^0 irregularity along the SC, $\sigma_t = 1.0$, $c = 0.9$, $N_x = N_y = 32$

to the discontinuities in the scattering source. However, perhaps surprisingly, the AD residual results in a superior angular L_2 effectivity in the domain, Fig. 8. While the AD residual-estimated error in the domain shares many of the same features as the TE residual-estimated error, the former is contained in a tighter range than the latter. The reason why the AD residual-estimated error is better than the TE residual-estimated error despite having more approximations is not clearly known, but this was consistently observed for a variety of cases examined, suggesting that perhaps this unexpected trend is not a fluke. One case where this is not true is where the optical thickness is large and derivative estimation is poor.

From Fig. 8 it is also clear that the worse estimation comes from points on or near the SC's and points that are surrounded by SC's. This is to be expected since the deviation incurred by poor approximation of the residual about SC's is not confined to the cells intersected by the SC's. When, during a transport sweep to solve for the approximated error, a significant deviation from the true residual is introduced by the SC, it is spread downwind in subsequent cell calculations. This contribution is relatively minor unless the SC's are prominent – i.e., the discontinuities are large – or other SC's have also contributed significantly to the inaccuracy of the residual in that cell.

4. Residual Source Estimator and Ragusa-Wang Estimator

We computed the error generated by the residual source estimator with approximated derivatives and compared it to the RW estimator on DGFEM-0 solutions for all combinations of the following cases: C^0 and C^1 irregularity along the SC, total cross-section $\sigma_t = [0.1, 1.0, 10.0]$, scattering ratio $c = [0.1, 0.6, 0.9]$, and number of cells $N_x = N_y = [4, 8, 16, 32, 64, 128]$. Results were varying, but the residual source estimator and RW estimator are generally competitive in terms of the effectivity. To highlight the varying results and overall competitiveness of the two methods, we select three cases for detailed exposition.

A. Case 1

Case 1 is the same as the previous examples presented in this paper: C^0 irregularity along the SC, $\sigma_t = 1.0$, and $c = 0.9$, but to get a clearer picture of the behaviour of the two estimators we increase the number of cells to $N_x = N_y = 128$. Figures 9 and 10 show $\log_{10}$-scale histogram plots of the local angular and scalar effectivity, respectively, of the residual source estimator. Color-coding is used to quantify the magnitude of the absolute difference between estimated and true error. We posited that in some cases poor estimation in a relative sense could be caused by minuscule true error, but this appears not to be true. Figures 11 and 12 show $\log_{10}$-

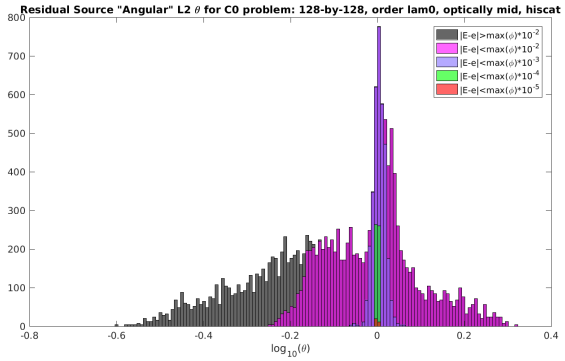

Fig. 9: Angular L_2 effectivity for residual source estimator; C^0 irregularity along the SC, $\sigma_t = 1.0$, $c = 0.9$, $N_x = N_y = 128$

scale histogram plots of the local angular and scalar effectivity, respectively, of the RW estimator.

Here we see some differences that are consistent for all comparisons between angular and scalar error norms for residual source and RW. Both scalar estimates result in tails that span many orders of magnitude, although the RW estimator

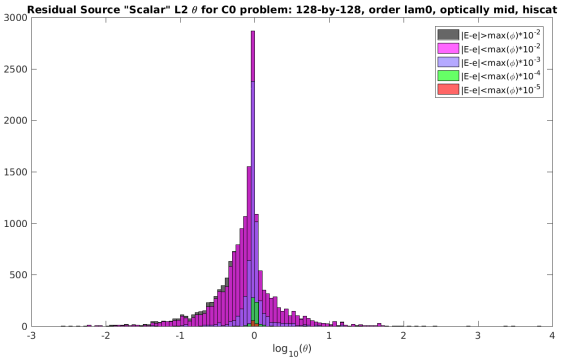

Fig. 10: Scalar L_2 effectivity for residual source estimator; C^0 irregularity along the SC, $\sigma_t = 1.0$, $c = 0.9$, $N_x = N_y = 128$

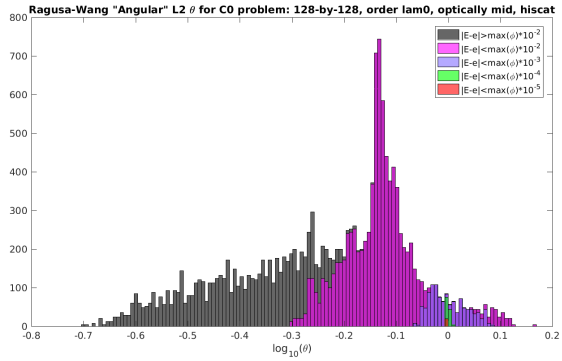

Fig. 11: Angular L_2 effectivity for RW estimator; C^0 irregularity along the SC, $\sigma_t = 1.0$, $c = 0.9$, $N_x = N_y = 128$

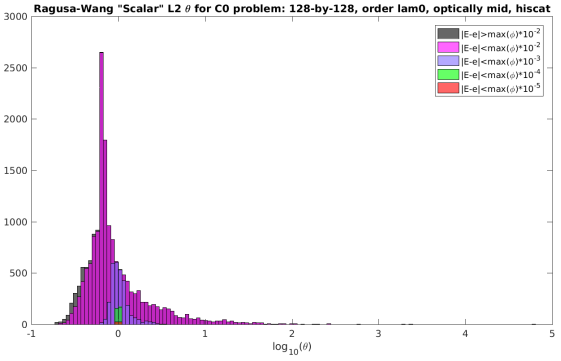

Fig. 12: Scalar L_2 effectivity for RW estimator; C^0 irregularity along the SC, $\sigma_t = 1.0$, $c = 0.9$, $N_x = N_y = 128$

tail favors overestimates. Also note that while these plots appear to show that scalar estimates increase the number of points in near perfect agreement, this is only due to widening bin widths in order to capture a wider range of effectivity values.

In this case, and generally, both forms of the RW estimator underestimate the true error, while the residual source estimator is more centered about the true value, although it does tend to favor underestimation slightly.

B. Case 2

Case 2 has C^1 irregularity along the SC, $\sigma_t = 10.0$, $c = 0.1$, and $N_x = N_y = 128$. This case was chosen as one favorable to the residual source estimator. Figures 13, 14, 15, and 16 show the angular residual source, scalar residual source, angular RW, and scalar RW effectivity results, respectively. In Case 2 both residual source estimator error norms

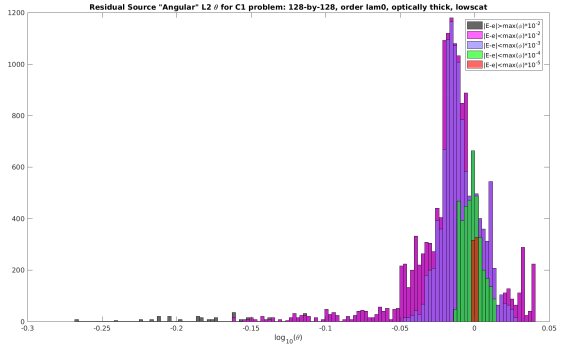

Fig. 13: Angular L_2 effectivity for residual source estimator; C^1 irregularity along the SC, $\sigma_t = 10.0$, $c = 0.1$, $N_x = N_y = 128$

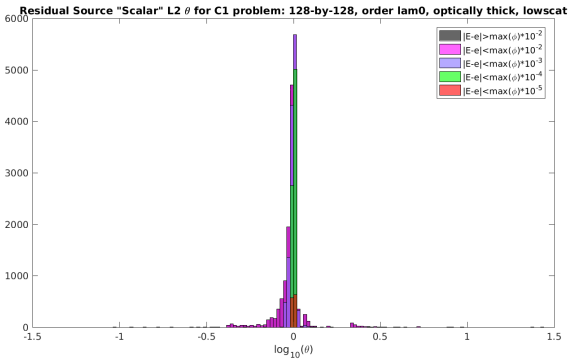

Fig. 14: Scalar L_2 effectivity for residual source estimator; C^1 irregularity along the SC, $\sigma_t = 10.0$, $c = 0.1$, $N_x = N_y = 128$

perform better than both RW estimator error norms. The residual source estimator angular effectivity has a peak at nearly exact and a second peak slightly underestimating the true error. The underestimate peak is due to the shortcomings of the Taylor expansion and derivative approximations.

C. Case 3

Case 3 is identical to Case 2 except the scattering ratio has been changed so that $c = 0.9$. Figures 17, 18, 19, and 20 show the angular residual source, scalar residual source, angular RW, and scalar RW effectivity results, respectively.

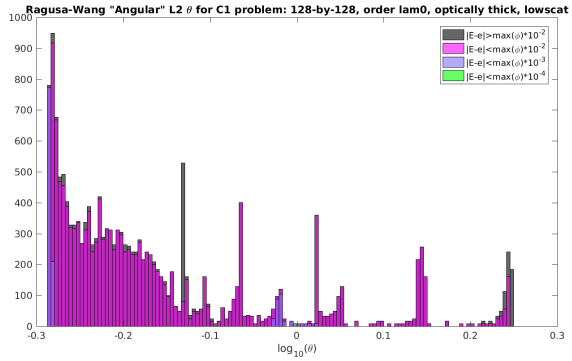

Fig. 15: Angular L_2 effectivity for RW estimator; C^1 irregularity along the SC, $\sigma_t = 10.0$, $c = 0.1$, $N_x = N_y = 128$

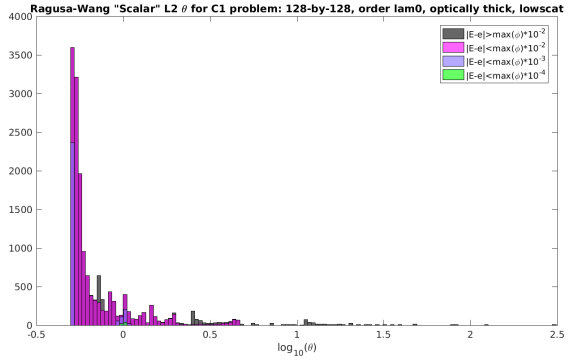

Fig. 16: Scalar L_2 effectivity for RW estimator; C^1 irregularity along the SC, $\sigma_t = 10.0$, $c = 0.1$, $N_x = N_y = 128$

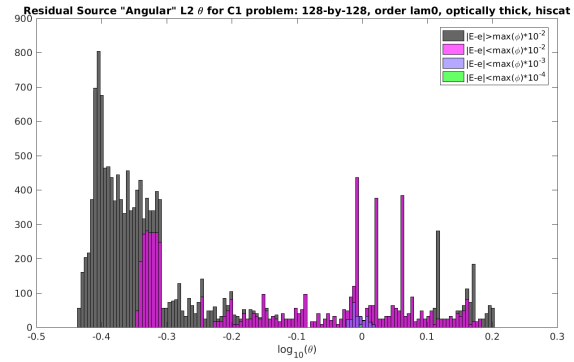

Fig. 17: Angular L_2 effectivity for residual source estimator; C^1 irregularity along the SC, $\sigma_t = 10.0$, $c = 0.9$, $N_x = N_y = 128$

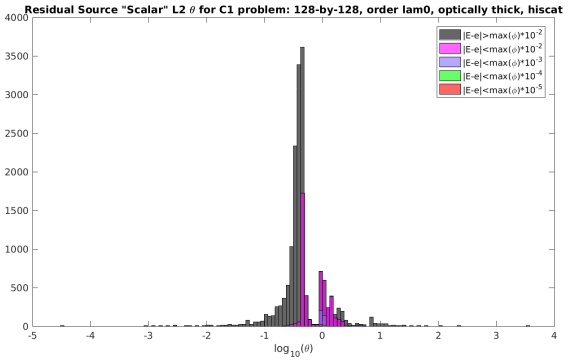

Fig. 18: Scalar L_2 effectivity for residual source estimator; C^1 irregularity along the SC, $\sigma_t = 10.0$, $c = 0.9$, $N_x = N_y = 128$

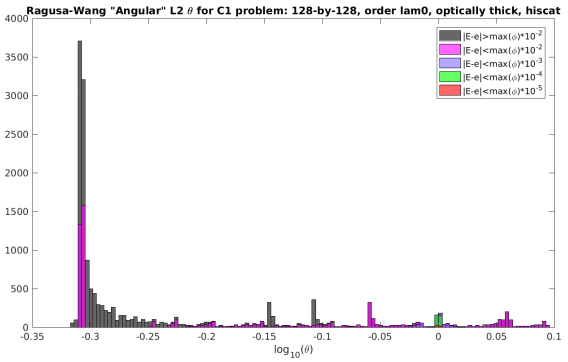

Fig. 19: Angular L_2 effectivity for RW estimator; C^1 irregularity along the SC, $\sigma_t = 10.0$, $c = 0.9$, $N_x = N_y = 128$

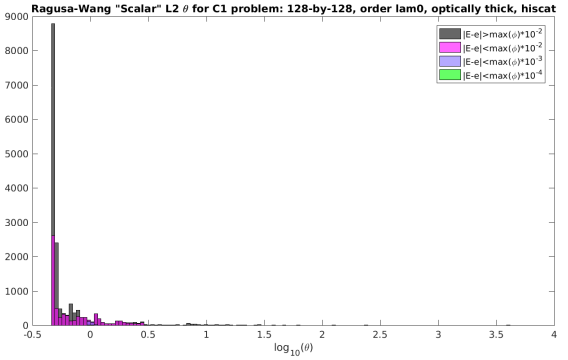

Fig. 20: Scalar L_2 effectivity for RW estimator; C^1 irregularity along the SC, $\sigma_t = 10.0$, $c = 0.9$, $N_x = N_y = 128$

This case highlights how poor approximation of the derivatives can hamper the residual source estimator when compared to the RW estimator. Poor derivative approximation is caused by the dual effect of a thick optical thickness which results in a rapidly changing true solution that the low-order approximation cannot capture and a large scattering ratio that increases the incorrect approximation of the angular flux derivative in other ordinates as well. RW does not have this issue, however, and it gives a precise, close underestimate of the solution.

IV. CONCLUSIONS AND DISCUSSION

The residual source estimator for DGFEM-0 has promising results. Despite poor estimation of the residual on the SC's and in the presence of steep gradients of the true solution, the angular form of the residual source estimator typically is contained within an order of magnitude in either direction about exact estimation. In conditions that are more favorable, the residual source estimator in the angular and scalar versions peaks near the exact value. A drawback in the scalar version, which the authors are aware is more readily applicable to most transport codes, is the presence of under and overestimation tails that, while diminishing quickly, extend several orders of magnitude away from the ideal effectivity unit value.

When compared to the RW estimator on the basis of quality of estimation, there are certain configurations where the RW estimator is advantageous, where the residual source estimator is advantageous, and where the two are competitive. One advantage of the RW estimator in all cases is that the scalar form of the RW estimator only exhibits an overestimation tail, meaning it is more conservative, and the tail does not span as many orders of magnitude in problems where the SC's adverse effects on the approximated residual are not as pronounced. The RW estimator in general is advantageous in situations where large gradients cause poor derivative approximation in the residual source estimator. The residual source estimator is advantageous in situations where this effect is suppressed. In general, though, the residual source estimator and RW estimator are competitive, particularly in the angular norm sense, and ultimately, given the estimators as presented in this work, there is no clear cut answer as to which estimator is preferable for a given case. However, the residual source estimator has the potential to nearly exactly estimate the true error for many of the cells, whereas even in situations extremely favorable to it, the RW estimator will reliably underestimate, in agreement with [6].

One aspect of the residual estimator that is intriguing is the fact that the exact residual produces exact error distributions and that the points at which the approximate residual deviates substantially from the exact residual are identifiable. This holds the potential for improving the derivative approximations and the approximation of the residual on the SC's that we conjecture will yield improvement of the error estimate distribution. This foundation will ultimately be used to approximate the residual on higher order DGFEM-Λ approximations.

V. ACKNOWLEDGMENTS

This material is based upon work supported under a Department of Energy, Office of Nuclear Energy, Integrated University Program Graduate Fellowship. Any opinions, findings, conclusions or recommendations expressed in this publication are those of the authors and do not necessarily reflect the views of the Department of Energy Office of Nuclear Energy. It was also supported under a National Academy for Nuclear Training Fellowship. The work of the second author (YYA) is supported by the Department of Energy National Nuclear Security Administration under Award Number *DENA0002576*.

Thanks are extended to Sean O'Brien and Sebastian Schunert for their willingness to correspond and offer assistance with the reported work.

REFERENCES

1. J. I. DUO, Y. Y. AZMY, and L. T. ZIKATANOV, "A posteriori error estimator and AMR for discrete ordinates nodal transport methods," *Annals of Nuclear Energy*, **36** (2009).
2. S. O'BRIEN and Y. Y. AZMY, "*A Posteriori* Error Estimators for the Discrete Ordinates Approximation of the One-Speed Neutron Transport Equation," in "*A Posteriori* Error Estimators for the Discrete Ordinates Approximation of the One-Speed Neutron Transport Equation," American Nuclear Society, LaGrange Park, IL, Sun Valley, Idaho, USA (May 5-9 2013), International Conference on Mathematics and Computational Methods Applied to Nuclear Science & Engineering (M&C 2013).
3. E. LEWIS and W. MILLER, JR., *Computational Methods of Neutron Transport*, American Nuclear Society, Inc. La Grange Park, Illinois USA (1993).
4. S. SCHUNERT and Y. Y. AZMY, "Comparison of the Accuracy of Various Spatial Discretization Schemes of the Discrete Ordinates Equations in 2D Cartesian Geometry," in "Comparison of the Accuracy of Various Spatial Discretization Schemes of the Discrete Ordinates Equations in 2D Cartesian Geometry," (2011), International Conference on Mathematics and Computational Methods Applied to Nuclear Science & Engineering (M&C 2011).
5. S. SCHUNERT and Y. AZMY, "Comparison of Spatial Discretization Methods for Solving the S_N Equations Using a Three-Dimensional Method of Manufactured Solutions Benchmark Suite with Escalating Order of Nonsmoothness," *Nuclear Science and Engineering*, **180**, 1–29 (2015).
6. S. O'BRIEN, *A Posteriori Error Estimators for the Discrete Ordinates Approximation of the One-Speed Neutron Transport Equation.*, Master's thesis, North Carolina State University (2012).
7. Y. WANG and J. C. RAGUSA, "Standard and goal-oriented adaptive mesh refinement applied to radiation transport on 2D unstructured triangular meshes," *Journal of Computational Physics*, **230** (2011).
8. Y. WANG and J. C. RAGUSA, "On the Convergence of DGFEM Applied to the Discrete Ordinates Transport Equation for Structured and Unstructured Triangular Meshes," *Nuclear Science and Engineering*, **163** (2009).